# Finite-difference time-domain modeling of curved material interfaces by using boundary condition equations method*

Jia Lu(卢佳) and Huaichun Zhou(周怀春)†

*Department of Thermal Engineering, Tsinghua University, Beijing* 100084, *China*

(Received 15 March 2016; revised manuscript received 12 May 2016; published online 2 August 2016)

To deal with the staircase approximation problem in the standard finite-difference time-domain (FDTD) simulation, the two-dimensional boundary condition equations (BCE) method is proposed in this paper. In the BCE method, the standard FDTD algorithm can be used as usual, and the curved surface is treated by adding the boundary condition equations. Thus, while maintaining the simplicity and computational efficiency of the standard FDTD algorithm, the BCE method can solve the staircase approximation problem. The BCE method is validated by analyzing near field and far field scattering properties of the PEC and dielectric cylinders. The results show that the BCE method can maintain a second-order accuracy by eliminating the staircase approximation errors. Moreover, the results of the BCE method show good accuracy for cylinder scattering cases with different permittivities.

**Keywords:** finite-difference time-domain, curved surface, staircase error, boundary condition equation

**PACS:** 02.60.–x, 02.70.–c, 41.20.Jb, 46.15.–x **DOI:** 10.1088/1674-1056/25/9/090203

## 1. Introduction

The interactions of electromagnetic waves with a curved surface have been widely discussed in many applications, such as material science, optics, photonic crystals, antenna design, and remote sensing.[1–6] In recent decades, a number of numerical methods have been reported for the interactions of electromagnetic waves with curved surfaces, including finite difference methods,[7,8] finite element methods,[9,10] and integral equation methods.[11,12] Among these methods, the finite-difference time-domain method is widely used in computational electrodynamics for easy implementation and accurate results.[13–17] When modeling a curved surface, however, the numerical accuracy may be reduced, because the standard FDTD algorithm uses staircase grids to approximate the material interface.[18] The staircase approximation, as depicted in Fig. 1, is generally adopted because of the discretization of the surface position. Obviously, the scattering properties of the curved surface will change going from the real shape to the staircase shape, especially if the mesh is coarse and the dielectric contrast is large.[19]

A possible solution to the staircase approximation problem is using non-orthogonal grids or curvilinear coordinates to approximate the curved surface.[20,21] Obviously, while improving the numerical accuracy, these methods would increase the complexity of the algorithm and cause numerical artifacts.[19] A more commonly used method is the conformal FDTD method.[22] However, the numerical stability of the contour-path FDTD method may not be guaranteed, because there are electric nodes whose values are borrowed from neighbor cells.[23] Research is ongoing for the improvements of the contour-path FDTD method based on the numerical instability problems.[23,24]

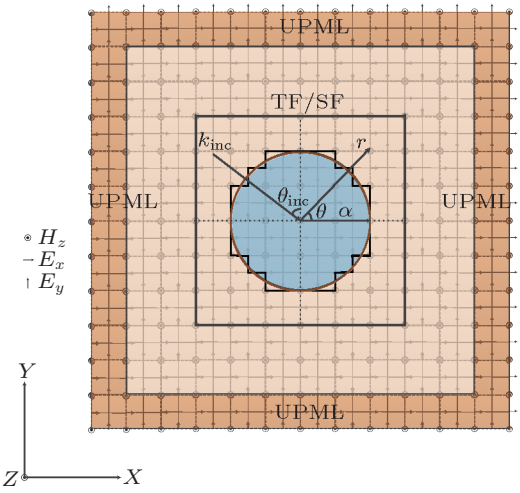



**Fig. 1.** (color online) Staircase approximation of a circular cylinder in FDTD calculation. Here, UPML means uniaxial perfectly matched layer. TF/SF: total field/scattering field.

Another possible way for solving the staircase approximation problem is using the effective permittivity to model the dielectric interface. There are several works presenting different kinds of effective permittivity methods, including the volume average method, a first-neighbor average method, the Maxwell–Garnett method, an inverted Maxwell–Garnett method, and the Bruggeman formula method.[19] The problem of the effective permittivity method resides in the selection of the most suitable effective permittivity value. There have been improvements to the effective permittivity method.[25,26] Among these improvements, the sub-pixel smoothing method

*Project supported by the National Natural Science Foundation of China (Grant No. 51025622).

†Corresponding author. E-mail: hczh@mail.tsinghua.edu.cn

© 2016 Chinese Physical Society and IOP Publishing Ltd 

shows second-order accuracy by employing the mean permittivity for surface-parallel electric components and the harmonic mean permittivity for surface-perpendicular electric components.[27,28]

A third approach is to simulate the real shape by considering the physical location of curved surfaces.[29,30] These methods show good accuracy and almost need no additional computational cost. However, the complexity of the algorithm would be increased due to the modification of the Yee algorithm. According to the classical electromagnetic theory, material interface boundary condition equations are essential for the scattering problems calculation.[31] Therefore, we utilize the Yee algorithm as usual and treat the surface interface as a kind of interface boundary. The layer of grids across the boundary is calculated by considering the boundary condition equations and physical location of the surface interface. Thus, while maintaining the simplicity and computational efficiency of the Yee scheme, the algorithm can solve the staircase approximation problem.

In this work, the boundary condition equations (BCE) method is utilized to deal with the staircase approximation problem in curved surface scattering. The paper is organized as follows. Firstly, the two-dimensional BCE algorithm is proposed in this paper. Subsequently, the BCE method is validated by analyzing the induced surface current on a PEC circular cylinder. Furthermore, the near field scattering properties of the dielectric circular cylinders are investigated, and the relative errors of different methods are compared. Then, we discuss the far field scattering properties of dielectric cylinders and show the effect of different dielectric permittivities on different methods. Finally, some concluding remarks are derived.

## 2. Numerical method

In this section, the BCE method is introduced to solve the staircase approximation problem in curved surface scattering.

### 2.1. Two-dimensional FDTD method

The finite difference time domain method is a state-of-the-art method for solving Maxwell's equations in complex geometries.[13] Considering linear, isotropic, non-dispersive, and lossy media, the FDTD method solves Maxwell's curl equations as follows:[13]

$$\frac{\partial \boldsymbol{E}}{\partial t} = \frac{1}{\varepsilon}\nabla \times \boldsymbol{H} - \frac{1}{\varepsilon}\left(\boldsymbol{J}_{\text{source}} + \sigma \boldsymbol{E}\right), \tag{1a}$$

$$\frac{\partial \boldsymbol{H}}{\partial t} = -\frac{1}{\mu}\nabla \times \boldsymbol{E} - \frac{1}{\mu}\left(\boldsymbol{M}_{\text{source}} + \sigma^{*} \boldsymbol{H}\right), \tag{1b}$$

where $\boldsymbol{E}$ and $\boldsymbol{H}$ are electric and magnetic field vectors, $\boldsymbol{J}_{\text{source}}$ and $\boldsymbol{M}_{\text{source}}$ are electric and magnetic sources, $\varepsilon$, $\mu$, $\sigma$, and $\sigma^{*}$ are electric permittivity, magnetic permeability, electric conductivity, and equivalent magnetic conductivity.

For TE wave incidence, Maxwell's equations in two-dimensional FDTD can be found in previous publications as[13]

$$\begin{aligned} & E_x^{n+1}(i+1/2, j) \\ &= C_a(m) E_x^n(i+1/2, j) + C_b(m) \\ &\quad \times \frac{H_z^{n+1/2}(i+1/2, j+1/2) - H_z^{n+1/2}(i+1/2, j-1/2)}{\Delta y}, \end{aligned} \tag{2a}$$

$$\begin{aligned} & E_y^{n+1}(i, j+1/2) \\ &= C_a(m) E_y^n(i, j+1/2) - C_b(m) \\ &\quad \times \frac{H_z^{n+1/2}(i+1/2, j+1/2) - H_z^{n+1/2}(i-1/2, j+1/2)}{\Delta x}, \end{aligned} \tag{2b}$$

$$\begin{aligned} & H_z^{n+1/2}(i+1/2, j+1/2) \\ &= D_a(m) H_z^n(i+1/2, j+1/2) - D_b(m) \\ &\quad \times \left[\frac{E_y^n(i+1, j+1/2) - E_y^n(i, j+1/2)}{\Delta x} \right. \\ &\quad \left. - \frac{E_x^n(i+1/2, j+1) - E_x^n(i+1/2, j)}{\Delta y}\right], \end{aligned} \tag{2c}$$

where

$$C_a(m) = \frac{2\varepsilon(m) - \sigma(m)\Delta t}{2\varepsilon(m) + \sigma(m)\Delta t}, \quad C_b(m) = \frac{2\Delta t}{2\varepsilon(m) + \sigma(m)\Delta t},$$

$$D_a(m) = \frac{2\mu(m) - \sigma^{*}(m)\Delta t}{2\mu(m) - \sigma^{*}(m)\Delta t}, \quad D_b(m) = \frac{2\Delta t}{2\mu(m) + \sigma^{*}(m)\Delta t}.$$

Two-dimensional FDTD equations for TM wave incidence can also be found in previous publications.[13]

### 2.2. Dielectric interface boundary condition

The FDTD computation setup is presented in Fig. 1. The FDTD calculation region is surrounded by the uniaxial perfectly matched layer (UPML) to simulate electromagnetic wave propagation outside the computation region without reflection. In the computation region, there are plane waves incident on the infinite cylinder. The plane waves are added by using the total field/scattering field (TF/SF) method.[13] As shown in Fig. 1, the FDTD computation region is divided by discrete grids. Within the grids, there are $H_z$, $E_x$, and $E_y$ components represented by circles and arrows. There are two regions painted by different colors. The two regions represent two kinds of materials. The red line between the two materials is the material interface, which is usually approximated by the black line with a staircase shape in FDTD simulations. By using the staircase approximation, electromagnetic wave scattering will change going from the real shape to the staircase shape, especially if the mesh is coarse and the dielectric contrast is large.[19] In order to make the material parameters change smoothly and improve the numerical accuracy, the averaged material parameters of adjacent grids have been used

by earlier researchers. Usually, there are two kinds of method, namely arithmetic mean and harmonic mean method,[32] they are

Arithmetic mean:[32]

$$\varepsilon_{\text{eff}} = \frac{\varepsilon_1 + \varepsilon_2}{2}, \quad \mu_{\text{eff}} = \frac{\mu_1 + \mu_2}{2}, \tag{3a}$$

Harmonic mean:[32]

$$\varepsilon_{\text{eff}} = \frac{2\varepsilon_1\varepsilon_2}{\varepsilon_1 + \varepsilon_2}, \quad \mu_{\text{eff}} = \frac{2\mu_1\mu_2}{\mu_1 + \mu_2}. \tag{3b}$$

However, these methods still suffer from the drawbacks of staircase approximation. To improve the numerical accuracy, the boundary condition equations on the material interface must be considered. For the curved surface case, we can use the same Yee algorithm as usual and just apply the boundary condition equations on the interface boundary. To calculate the grids across the interface boundary, the physical location of the interface boundary must be considered rigorously.[29]

Figure 2 shows the electromagnetic fields configuration near the material interface. Consider the scheme for updating the $H_z$ field, the magnetic field point and the nearest four electric field points are treated as a group. When an interface passes through the group of points, it separates some electric fields and the magnetic field into different media. In Fig. 2, for example, the material interface intersects one line connecting $E_y(i, j+1/2)$ and $H_z(i+1/2, j+1/2)$ at point Int1 and another line connecting $E_x(i+1/2, j+1)$ and $H_z(i+1/2, j+1/2)$ at point Int2. Thus, $E_x(i+1/2, j+1)$ and $E_y(i, j+1/2)$ are separated from the other three components. Here, $\varphi_x$ denotes the ratio of the distance between point Int1 and $H_z(i+1/2, j+1/2)$ to the distance between $H_z(i-1/2, j+1/2)$ and $H_z(i+1/2, j+1/2)$. $\varphi_y$ denotes the ratio of the distance between point Int2 and $H_z(i+1/2, j+1/2)$ to the distance between $H_z(i+1/2, j+3/2)$ and $H_z(i+1/2, j+1/2)$. $E_{\text{T}}(\text{int}1_1)$ and $E_{\text{N}}(\text{int}1_1)$ are the tangential and normal components of the electric field respectively at point Int1; $E_{\text{T}}(\text{int}2_1)$ and $E_{\text{N}}(\text{int}2_1)$ are those components at point Int2. In addition, it can be seen from Fig. 2 that the surface interface makes an angle of $\alpha$ with the $x$ direction.

To update $H_z(i+1/2, j+1/2)$ in Fig. 2, both $E_x^n(i+1/2, j+1)$ and $E_y^n(i, j+1/2)$ in Eq. (2c) must be replaced by new values of $E_x^n(i+1/2, j+1)$ and $E_y^n(i, j+1/2)$ in medium 2. The new $E_y^n(i, j+1/2)$ in medium 2 can be approximated as

$$\begin{aligned} &E_y^n(\text{int}1_2) - E_y^n(i+1, j+1/2) \\ &= (0.5+\varphi_x)\left[E_y^n(i, j+1/2) - E_y^n(i+1, j+1/2)\right], \end{aligned} \tag{4}$$

i.e.,

$$E_y^n(i, j+1/2) = \frac{E_y^n(\text{int}1_2) - (0.5-\varphi_x)E_y^n(i+1, j+1/2)}{(0.5+\varphi_x)}. \tag{5}$$

Here, $\text{int}1_2$ means that the point is just below the boundary interface in media 2. For grids across the boundary, coefficients of $C_{\text{a}}$, $C_{\text{b}}$, $D_{\text{a}}$, and $D_{\text{b}}$ in Eq. (2) are calculated based on the location of the boundary. To determine the location of the boundary, the surface location, intersection ratio, and surface slope angle are calculated in the preprocessing stage.

Similarly, the formula of the new $E_x^n(i+1/2, j+1)$ is

$$E_x^n(i+1/2, j+1) = \frac{E_x^n(\text{int}2_2) - (0.5-\varphi_y)E_x^n(i+1/2, j)}{(0.5+\varphi_y)}, \tag{6}$$

where $E_y^n(\text{int}1_2)$ and $E_x^n(\text{int}2_2)$ in Eqs. (4)–(6) are unknown parameters, which can be calculated by the boundary condition equations near the material interface. Boundary condition equations at the dielectric interface state that the tangential component of the electric field is continuous across the boundary, whereas the normal component of the electric field changes discontinuously across the boundary.[31] The calculation of $E_x^n(\text{int}2_{\text{d}})$ will be shown by applying boundary condition equations.

According to the forward difference approximation with the first-order accuracy, we obtain

$$\frac{\partial E_x^n(i+1/2, j)}{\partial y} = \frac{[E_x^n(i+1/2, j+1) - E_x^n(i+1/2, j)]}{\text{d}y}, \tag{7}$$

and based on the forward difference approximation with the second-order accuracy, we obtain

$$\frac{\partial E_x^n(i+1/2, j)}{\partial y} = \frac{[-E_x^n(i+1/2, j+2) + 4E_x^n(i+1/2, j+1) - 3E_x^n(i+1/2, j)]}{2\cdot \text{d}y}. \tag{8}$$

Substituting Eq. (8) into Eq. (7), we can obtain

$$\begin{aligned} &E_x^n(i+1/2, j) \\ &= 2E_x^n(i+1/2, j+1) - E_x^n(i+1/2, j+2), \end{aligned} \tag{9}$$

and then, $E_x^n(\text{int}2_1)$ can be approximated as

$$\begin{aligned} &E_x^n(\text{int}2_1) - E_x^n(i+1/2, j+1) \\ &= (0.5-\varphi_y)\left[E_x^n(i+1/2, j) - E_x^n(i+1/2, j+1)\right] \\ &= (0.5-\varphi_y)\left[E_x^n(i+1/2, j+1) - E_x^n(i+1/2, j+2)\right], \end{aligned} \tag{10}$$

i.e.,

$$\begin{aligned} E_x^n(\text{int}2_1) &= (1.5-\varphi_y)E_x^n(i+1/2, j+1) \\ &\quad - (0.5-\varphi_y)E_x^n(i+1/2, j+2). \end{aligned} \tag{11}$$

Here, int$2_1$ means that the point is just above the boundary interface in media 1.

Similarly, the formula of $E_y^n(\text{int}2_1)$ is

$$\begin{aligned} & E_y^n(\text{int}2_1) \\ = \; & 1.5\left[(1-\varphi_y)E_y^n(i,j+1/2)+\varphi_y E_y^n(i,j+3/2)\right] \\ & -0.5\left[(1-\varphi_y)E_y^n(i-1,j+1/2)\right. \\ & \left.+\varphi_y E_y^n(i-1,j+3/2)\right]. \end{aligned} \tag{12}$$

With $E_x^n(\text{int}2_1)$ and $E_y^n(\text{int}2_1)$ known, we can derive $E_{\text{N}}^n(\text{int}2_1)$ and $E_{\text{T}}^n(\text{int}2_1)$ using coordinates transformation

$$\begin{aligned} \begin{pmatrix} E_{\text{N}}^n(\text{int}2_1) \\ E_{\text{T}}^n(\text{int}2_1) \end{pmatrix} &= \begin{pmatrix} \cos\alpha & \sin\alpha \\ -\sin\alpha & \cos\alpha \end{pmatrix} \cdot \begin{pmatrix} E_x^n(\text{int}2_1) \\ E_y^n(\text{int}2_1) \end{pmatrix} \\ &= R \cdot \begin{pmatrix} E_x^n(\text{int}2_1) \\ E_y^n(\text{int}2_1) \end{pmatrix}. \end{aligned} \tag{13}$$

To calculate $E_{\text{N}}^n(\text{int}2_2)$ and $E_{\text{T}}^n(\text{int}2_2)$, the boundary condition equations at the dielectric interface should be applied as[33]

$$\begin{aligned} & \boldsymbol{n}\times(\boldsymbol{E}_2-\boldsymbol{E}_1)=\boldsymbol{0}, \quad \boldsymbol{n}\times(\boldsymbol{H}_2-\boldsymbol{H}_1)=\boldsymbol{0}, \\ & \boldsymbol{n}\cdot(\boldsymbol{D}_2-\boldsymbol{D}_1)=0, \quad \boldsymbol{n}\cdot(\boldsymbol{B}_2-\boldsymbol{B}_1)=0, \end{aligned} \tag{14}$$

where $\boldsymbol{D}=\varepsilon\boldsymbol{E}$ and $\boldsymbol{B}=\mu\boldsymbol{H}$ are the electric flux density and magnetic flux density.

Then, $E_{\text{N}}^n(\text{int}2_2)$ and $E_{\text{T}}^n(\text{int}2_2)$ can be calculated as

$$\begin{aligned} \begin{pmatrix} E_{\text{N}}^n(\text{int}2_2) \\ E_{\text{T}}^n(\text{int}2_2) \end{pmatrix} &= \begin{pmatrix} \varepsilon_1/\varepsilon_2 & 0 \\ 0 & 1 \end{pmatrix} \cdot \begin{pmatrix} E_{\text{N}}^n(\text{int}2_1) \\ E_{\text{T}}^n(\text{int}2_1) \end{pmatrix} \\ &= T \cdot \begin{pmatrix} E_{\text{N}}^n(\text{int}2_1) \\ E_{\text{T}}^n(\text{int}2_1) \end{pmatrix}. \end{aligned} \tag{15}$$

In addition,

$$\begin{pmatrix} E_x^n(\text{int}2_2) \\ E_y^n(\text{int}2_2) \end{pmatrix} = \boldsymbol{R}^{-1} \cdot \begin{pmatrix} E_{\text{N}}^n(\text{int}2_2) \\ E_{\text{T}}^n(\text{int}2_2) \end{pmatrix}. \tag{16}$$

Therefore, the boundary condition equations for material interface can be simplified as

$$\begin{pmatrix} E_x^n(\text{int}2_2) \\ E_y^n(\text{int}2_2) \end{pmatrix} = \boldsymbol{R}^{-1}\boldsymbol{T}\boldsymbol{R} \begin{pmatrix} E_x^n(\text{int}2_1) \\ E_y^n(\text{int}2_1) \end{pmatrix}, \tag{17}$$

where the matrices $\boldsymbol{R}$ and $\boldsymbol{T}$ are defined as

$$\boldsymbol{R} = \begin{pmatrix} \cos\alpha & \sin\alpha \\ -\sin\alpha & \cos\alpha \end{pmatrix}, \quad \boldsymbol{T} = \begin{pmatrix} \varepsilon_1/\varepsilon_2 & 0 \\ 0 & 1 \end{pmatrix}. \tag{18}$$

Thus, we derive the formulas of $E_x^n(\text{int}2_2)$ based on boundary condition equations. Similarly, $E_y^n(\text{int}1_2)$ can be calculated. Then, the $H_z(i+1/2,j+1/2)$ field is updated according to Eq. (2c). Here, new values of $E_x^n(i+1/2,j+1)$ and $E_y^n(i,j+1/2)$ in medium 2 are utilized in Eq. (2c). Parameters of medium 2 are used in $D_a$ and $D_b$.

Consider the scheme of updating the $E_x(i+1/2,j+1)$ field, the electric field point and the nearest two magnetic field points are treated as a group. When an interface passes through the group of points, it separates one magnetic field and the electric field into different media. The configuration can be presented in Fig. 2.

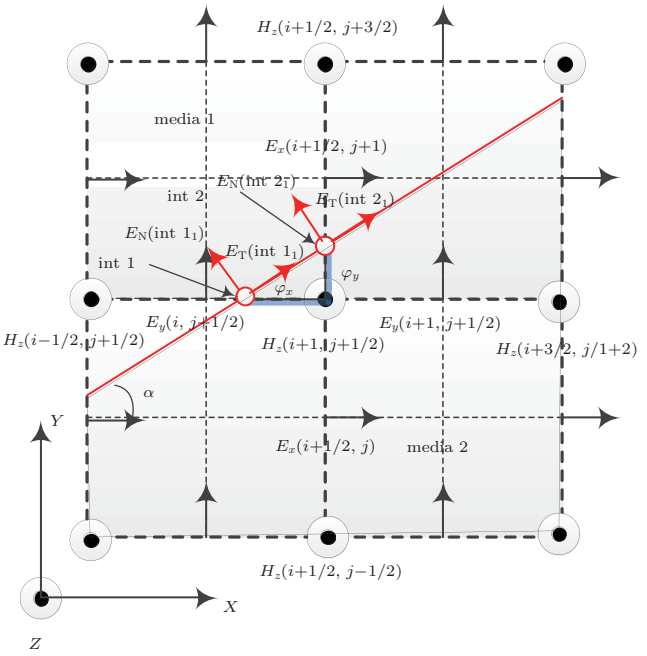



**Fig. 2.** (color online) Electromagnetic fields configuration for the material interface. Here, $E_{\text{T}}$ and $E_{\text{N}}$ are the tangential and normal components of the electric field.

To update $E_x(i+1/2,j+1)$ in Fig. 2, $H_z^{n+1/2}(i+1/2,j+1/2)$ in Eq. (2a) must be replaced by a new value of $H_z^{n+1/2}(i{+}1/2,\ j{+}1/2)$ in medium 1.

$$\begin{aligned} & H_z^{n+1/2}(i+1/2,j+1/2)-H_z^{n+1/2}(\text{int}2_1) \\ = \; & \varphi_y\left[H_z^{n+1/2}(i+1/2,j+1/2)\right. \\ & \left.-H_z^{n+1/2}(i+1/2,j+3/2)\right], \end{aligned} \tag{19}$$

i.e.,

$$\begin{aligned} & H_z^{n+1/2}(i+1/2,j+1/2) \\ = \; & \frac{H_z^{n+1/2}(\text{int}2_1)-\varphi_y H_z^{n+1/2}(i+1/2,j+3/2)}{(1-\varphi_y)}. \end{aligned} \tag{20}$$

Here, $H_z^{n+1/2}(\text{int}2_1)$ is an unknown parameter, which can be calculated by applying the boundary condition equations in Eq. (14) as

$$\begin{aligned} & H_z^{n+1/2}(\text{int}2_2)-H_z^{n+1/2}(i+1/2,j+1/2) \\ = \; & \varphi_y\left[H_z^{n+1/2'}(i+1/2,j+3/2)-H_z^{n+1/2}(i+1/2,j+1/2)\right] \\ = \; & \varphi_y\left[H_z^{n+1/2}(i+1/2,j+1/2)\right. \\ & \left.-H_z^{n+1/2}(i+1/2,j-1/2)\right], \end{aligned} \tag{21}$$

i.e.,

$$\begin{aligned} H_z^{n+1/2}(\text{int}2_1) &= \frac{\mu_2}{\mu_1}H_z^{n+1/2}(\text{int}2_2) \\ &= \frac{\mu_2}{\mu_1}\left[(1+\varphi_y)H_z^{n+1/2}(i+1/2,j+1/2)\right. \\ &\quad \left.-\varphi_y H_z^{n+1/2}(i+1/2,j-1/2)\right]. \end{aligned} \tag{22}$$

The scheme for updating the $E_y(i,j+1/2)$ field in Fig. 2 is the same as that of the $E_x(i+1/2,j+1)$ field, $H_z^n(i+1/2,j+1/2)$

in Eq. (2b) is replaced by the new value of $H_z^n(i+1/2, j+1/2)$ in medium 1.

### 2.3. PEC interface boundary condition

In the case of a PEC interface, the boundary condition equations are different from that of the dielectric interface. Assuming media 2 in Fig. 2 is PEC, the boundary condition equations become[33]

$$\boldsymbol{n} \times \boldsymbol{E}_1 = \boldsymbol{0}, \quad \boldsymbol{n} \cdot \boldsymbol{B}_1 = 0, \quad \boldsymbol{E}_2 = \boldsymbol{0}, \quad \boldsymbol{B}_2 = \boldsymbol{0}. \tag{23}$$

Then, $H_z(i+1/2, j+1/2) = 0$.

To update $E_x(i+1/2, j+1)$ in Fig. 2, $H_z^{n+1/2}(i+1/2, j+1/2)$ in Eq. (2a) must be replaced by a new value of $H_z^{n+1/2}(i+1/2, j+1/2)$ in medium 1.

$$\begin{aligned} & H_z^{n+1/2}(i+1/2, j+1/2) - H_z^{n+1/2}(\mathrm{int}2_1) \\ = \; & \varphi_y \left[ H_z^{n+1/2}(i+1/2, j+1/2) \right. \\ & \left. - H_z^{n+1/2}(i+1/2, j+3/2) \right], \end{aligned} \tag{24}$$

i.e.,

$$\begin{aligned} & H_z^{n+1/2}(i+1/2, j+1/2) \\ = \; & \frac{H_z^{n+1/2}(\mathrm{int}2_1) - \varphi_y H_z^{n+1/2}(i+1/2, j+3/2)}{(1-\varphi_y)}. \end{aligned} \tag{25}$$

Here, $H_z^{n+1/2}(\mathrm{int}2_1)$ is an unknown parameter, which can be calculated by applying the boundary condition equations in Eq. (23),

$$\begin{aligned} & H_z^{n+1/2}(\mathrm{int}2_1) - H_z^{n+1/2}(i+1/2, j+3/2) \\ = \; & (1-\varphi_y) \left[ H_z^{n+1/2}(i+1/2, j+1/2) \right. \\ & \left. - H_z^{n+1/2}(i+1/2, j+3/2) \right] \\ = \; & (1-\varphi_y) \left[ H_z^{n+1/2}(i+1/2, j+3/2) \right. \\ & \left. - H_z^{n+1/2}(i+1/2, j+5/2) \right], \end{aligned} \tag{26}$$

i.e.,

$$\begin{aligned} & H_z^{n+1/2}(\mathrm{int}2_1) \\ = \; & (2-\varphi_y) H_z^{n+1/2}(i+1/2, j+3/2) \\ & - (1-\varphi_y) H_z^{n+1/2}(i+1/2, j+5/2). \end{aligned} \tag{27}$$

The scheme for updating the $E_y(i, j+1/2)$ field in Fig. 2 is the same as that of the $E_x(i+1/2, j+1)$ field, $H_z^{n+1/2}(i+1/2, j+1/2)$ in Eq. (2b) is replaced by the new value of $H_z^{n+1/2'}(i+1/2, j+1/2)$ in medium 1.

Thus, we have set up the methodology for adding the boundary condition equations in a two-dimensional TE FDTD algorithm. In summary, the flow chart of the BCE method is drawn in Fig. 3. Similarly, we can derive the methodology for adding the boundary condition equations in the two-dimensional TM FDTD algorithm.

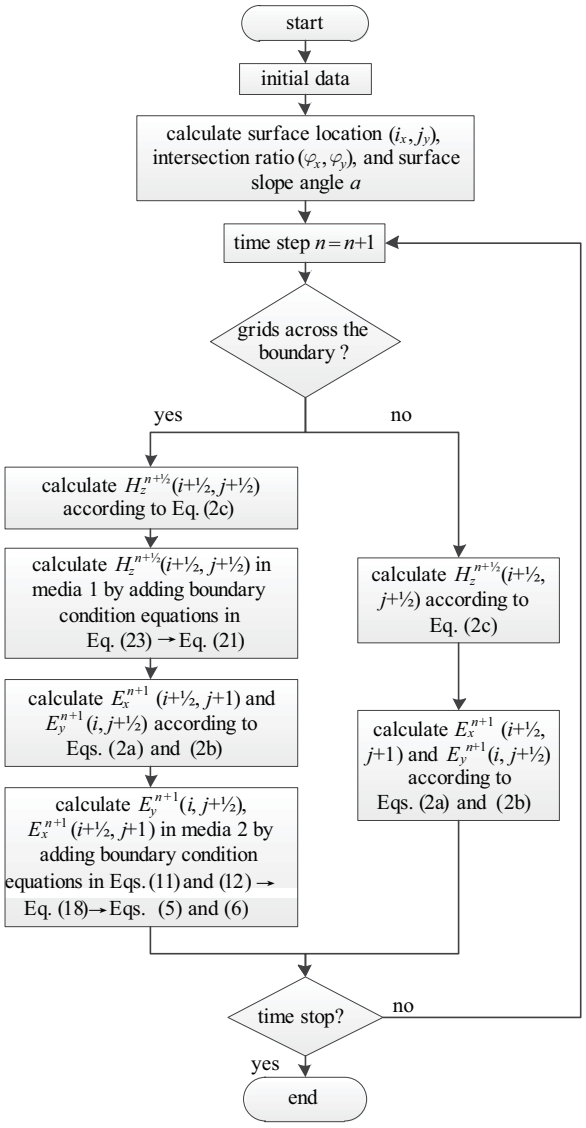



**Fig. 3.** Flow chart of the boundary condition equations method.

The BCE method utilizes the standard FDTD algorithm with a second-order accuracy. All the approximations across the boundary are based on the one side difference approximation or non-centered difference approximation. Thus, it is sufficient to guarantee a second-order accuracy globally.[30] In addition, the BCE method can be extended to solve three-dimensional problems. The surface location $(i, j, k)$ and intersection ratio $(\varphi_x, \varphi_y, \varphi_z)$ should be calculated instead of the surface location $(i, j)$ and intersection ratio $(\varphi_x, \varphi_y)$ in the preprocessing stage, also, matrix $R$ and $T$ must be replaced by a coordinate transform matrix in three dimensions. The boundary condition equations are similar to those of two-dimensional problems.

## 3. Results and discussion

In this section, analytical and numerical data validations of the BCE method are presented. Comparisons of different methods are made, including the staircase approxima-

tion (SA) method, arithmetic mean (AM) method, analytical solution (AS) method, and BCE method. Results from the sub-pixel smoothing (SPS) method are also given for method validation.[27,28]

### 3.1. PEC circular cylinder

To validate the FDTD algorithm, the induced surface current of a PEC circular cylinder is analyzed. The PEC circular cylinder has a radius of $a = 5/k_i$ and is under transverse electric (TE) illumination. Here, $k_i = 2\pi/\lambda$ is the wave vector. Figure 4 is a plot of the BCE method predicted surface currents and the SA method predicted surface currents compared to the reference data.[22] It can be seen from Fig. 4 that the BCE method predicted surface currents agree well with the series solution and contour FDTD results, whereas the SA method predicted surface currents do not agree well with the reference data.

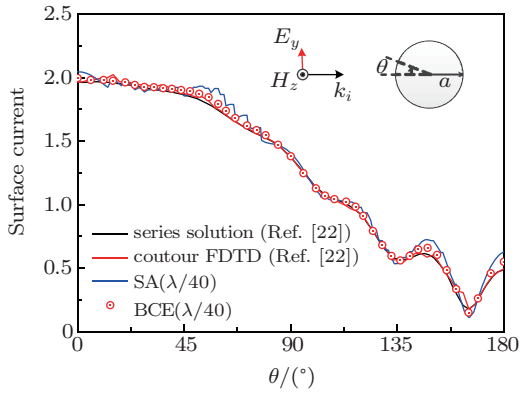



**Fig. 4.** (color online) Surface induced currents comparison. Series solution and contour FDTD are reference data. SA and BCE are staircase approximation and boundary condition equations method.

### 3.2. Dielectric circular cylinder, near field

In this part, the near field scattering properties of a $k_i a = 5$ dielectric circular cylinder is analyzed. The permittivity and permeability in free space are given as $\varepsilon_0 = 1$, $\mu_0 = 1$, $\sigma_0 = 0$, and $\sigma_{m,0} = 0$. The material parameters of the dielectric circular cylinder are $\varepsilon_d = 2$, $\mu_d = 1$, $\sigma_d = 0$, and $\sigma_{m,d} = 0$. The incident waves are time-harmonic TE mode fields with an amplitude of $|H_{in}| = 1.0$ A/m and transverse magnetic (TM) mode fields with an amplitude of $|E_{in}| = 1.0$ V/m. The incident waves have a wavelength of $\lambda = 1$ m. The grid size is chosen as $\lambda/160$, and the simulation time is chosen to be $t = 1.67 \times 10^{-7}$ s to make sure that the numerical results are convergent. We use the SA, BCE, and AS methods to calculate a total field region of $[-2:2]$ m$\times[-2:2]$ m. For the infinite cylinder scattering cases, analytical solutions can be derived from previous publications.[33–35]

To compare the local error in the whole computation region, the normalized L2 error for TE wave incidence can be defined as

$$\text{error} = \frac{\left[\iint (H_{sa} - H_{as})^2 \, dx dy\right]^{1/2}}{\left[\iint (H_{as})^2 \, dx dy\right]^{1/2}} \approx \frac{\left[\sum (H_{sa} - H_{as})^2\right]^{1/2}}{\left[\sum (H_{as})^2\right]^{1/2}}. \quad (28)$$

The normalized L2 error for TM wave incidence is similar to that for TE wave incidence.

Figure 5 shows normalized L2 errors of the BCE method predicted total field amplitude and the SA and AM methods-predicted total field amplitude. It can be seen from Fig. 5 that the SA, AM, and BCE methods are convergent with the decrease of the grid size for both TE and TM illuminations. The BCE method can maintain a second-order accuracy by eliminating the staircase approximation error, whereas the SA and AM method can only achieve a first-order accuracy. For the TE wave incidence, the BCE method with a grid size of $\lambda/40$ is good enough to achieve a better accuracy than the SA method with a grid size of $\lambda/160$. For the TM wave incidence, the SA and AM methods have the same normalized L2 error, because there are no magnetic permeability differences between the circular cylinder and air.

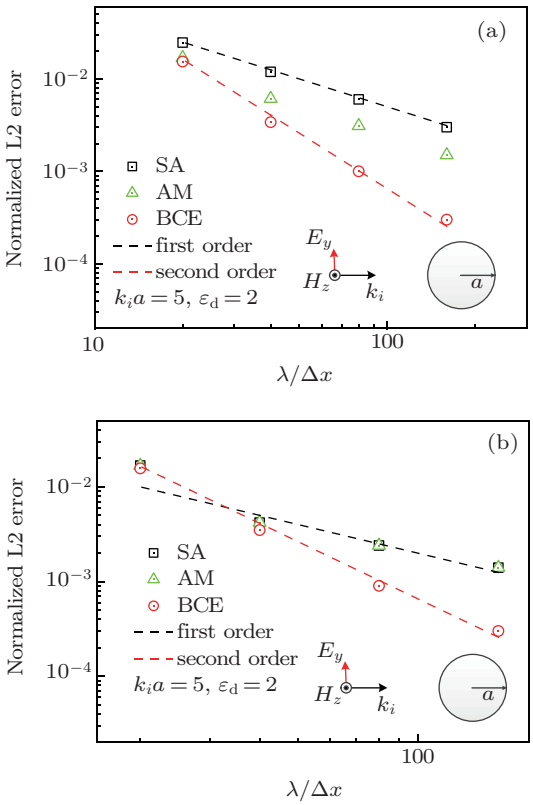



**Fig. 5.** (color online) The normalized L2 errors for plane wave incidence on the dielectric cylinder. SA, AM, and BCE are staircase approximation, arithmetic mean, and boundary condition equations method, respectively. (a) TE wave illumination and (b) TM wave illumination.

### 3.3. Multilayer dielectric cylinder, near field

In addition, the BCE method can be used to deal with multilayer object scattering problems. For the multilayer circular cylinder scattering cases, analytical solutions can be derived based on the Mie theory.[36,37] In this part, the near field scattering properties of two double-layer dielectric circular cylinders is analyzed. The radius of the first double-layer circular cylinder is $a = 5/(2\pi)$ m and $a_i = 5/(4\pi)$ m. The radius of the second double-layer circular cylinder are $a = 15/(2\pi)$ m and $a_i = 15/(4\pi)$ m. The material parameters of the outer dielectric circular cylinders are $\varepsilon_{\rm d} = 2$, $\mu_{\rm d} = 1$, $\sigma_{\rm d} = 0$, and $\sigma_{\rm m,d} = 0$. The material parameters of the inner dielectric circular cylinders are $\varepsilon_{\rm d,i} = 4$, $\mu_{\rm d} = 1$, $\sigma_{\rm d,i} = 0$, and $\sigma_{\rm m,d,i} = 0$. The incident waves have a wavelength of $\lambda = 1$ m. We use the SA, BCE, SPS, and AS methods to calculate a total field region of $[-2:2]$ m$\times[-2:2]$ m.

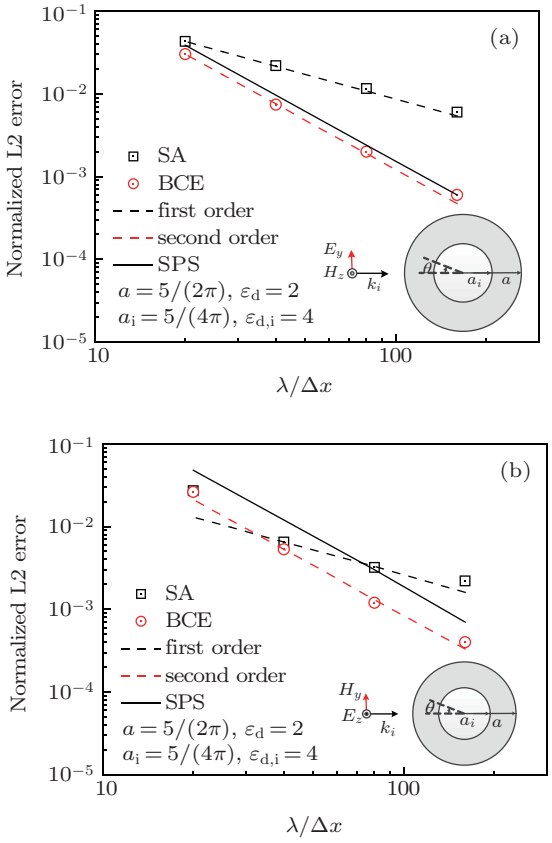



**Fig. 6.** (color online) The normalized L2 errors for plane wave incidence on the double layer dielectric cylinder ($a = 5/(2\pi), a_i = 5/(4\pi)$). SA, BCE, and SPS are staircase approximation, boundary condition equations, and sub-pixel smoothing method, respectively. (a) TE wave illumination and (b) TM wave illumination.

Figures 6 and 7 show normalized L2 errors of the BCE method predicted total field amplitude and the SA and SPS methods-predicted total field amplitude. It can be seen from the two figures that the BCE and SPS methods can maintain a second-order accuracy by eliminating the staircase approximation error, whereas the SA method can only achieve a first-order accuracy. Meanwhile, it can be seen from the two figures that the results of the BCE method show better accuracy than that of the SPS method. The reason is that the BCE method is able to consider the physical location of curved surfaces according to the surface location and intersection ratio. Comparing Fig. 6 with Fig. 7, it can be seen that the results of the BCE and SPS methods show less improvements of the staircase errors for larger structures. The reason is that the dielectric interface becomes smoother with the increase of the structure size.

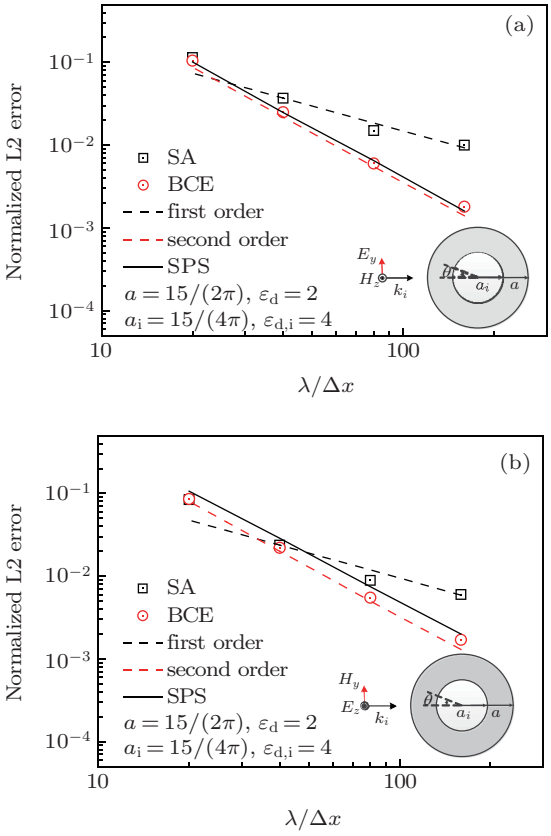



**Fig. 7.** (color online) The normalized L2 errors for plane wave incidence on the double layer dielectric cylinder ($a = 15/(2\pi), a_i = 15/(4\pi)$). SA, BCE, and SPS are staircase approximation, boundary condition equations, and sub-pixel smoothing methods, respectively. (a) TE wave illumination and (b) TM wave illumination.

### 3.4. Dielectric circular cylinder, far field

To compare the performance of the SA method and BCE method, the far field RCS of a dielectric circular cylinder with $a = 0.2\lambda$ is analyzed. The permittivity and permeability in free space are given as $\varepsilon_0 = 1$, $\mu_0 = 1$, $\sigma_0 = 0$, and $\sigma_{\rm m,0} = 0$. The material parameters of the dielectric circular cylinder are $\varepsilon_{\rm d} = 9$, $\mu_{\rm d} = 1$, $\sigma_{\rm d} = 0$, and $\sigma_{\rm m,d} = 0$. The incident waves are time-harmonic TE mode fields with an amplitude of $|H_{\rm in}| = 1.0$ A/m and TM mode fields with an amplitude of $|E_{\rm in}| = 1.0$ V/m. The incident waves have a wavelength of $\lambda = 1$ m. The grid size is chosen as $\lambda/80$, and the simulation time is chosen to be $t = 1.25 \times 10^{-8}$ s to make sure that the numerical results are convergent. We use the SA, BCE, and analytical solution methods to calculate the far field RCS.

Figure 8 shows the BCE method predicted RCS and the SA method predicted RCS compared with the analytical solution results. Obviously, the results of the BCE method agree well with those of the analytical solution method for large dielectric contrast cases. It can be seen from Fig. 8 that the results of the SA method with a grid size of $\lambda/80$ do not agree well with the analytical solution results for the large dielectric contrast case. The reason is that the scattering properties of a curved surface will change going from the real shape to the staircase shape, especially if the mesh is coarse and the dielectric contrast is large.[19] Meanwhile, the results of the SA method show better agreement with the analytical solution results with a smaller grid size of $\lambda/320$.

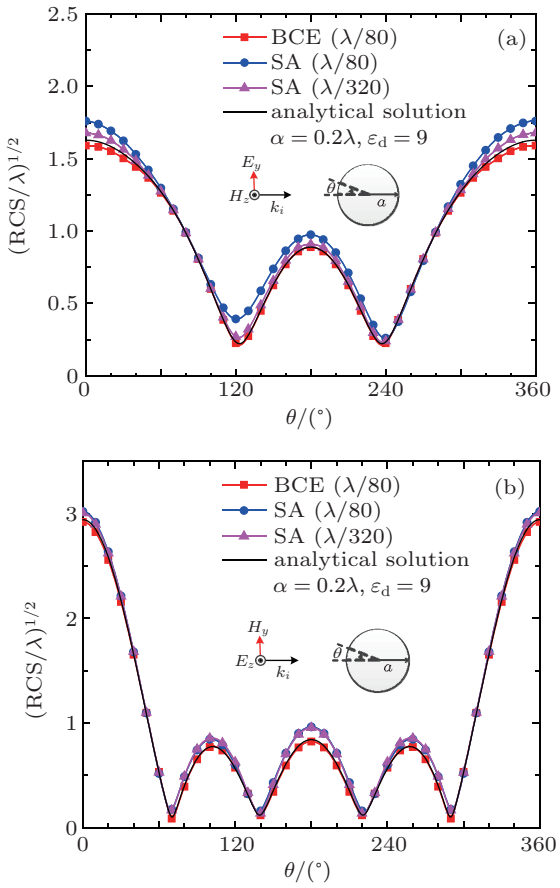



**Fig. 8.** (color online) Far field RCS comparison ($a = 0.2\lambda$, $\varepsilon_{\rm d} = 9$). SA and BCE are staircase approximation and boundary condition equations methods. (a) TE wave illumination and (b) TM wave illumination.

To demonstrate the method capability, the far field RCS of two cylinders with complex geometries are analyzed. The two cylinders are presented in Figs. 9 and 10. The cylinder in Fig. 9 has a square shape with $a = \lambda$, and the cylinder in Fig. 10 is a combination of a circular cylinder and a rectangle cylinder. The material parameters of the two cylinders are $\varepsilon_{\rm d} = 9$, $\mu_{\rm d} = 1$, $\sigma_{\rm d} = 0$, and $\sigma_{\rm m,d} = 0$. The incident waves have a wavelength of $\lambda = 1$ m. The grid size is chosen as $\lambda/80$, and the simulation time is chosen to be $t = 1.67 \times 10^{-7}$ s to make sure that the numerical results are convergent. We use the SA and BCE methods to calculate the far field RCS, and results of the MOM method are used as the benchmark for the comparison with the FDTD results.[35]

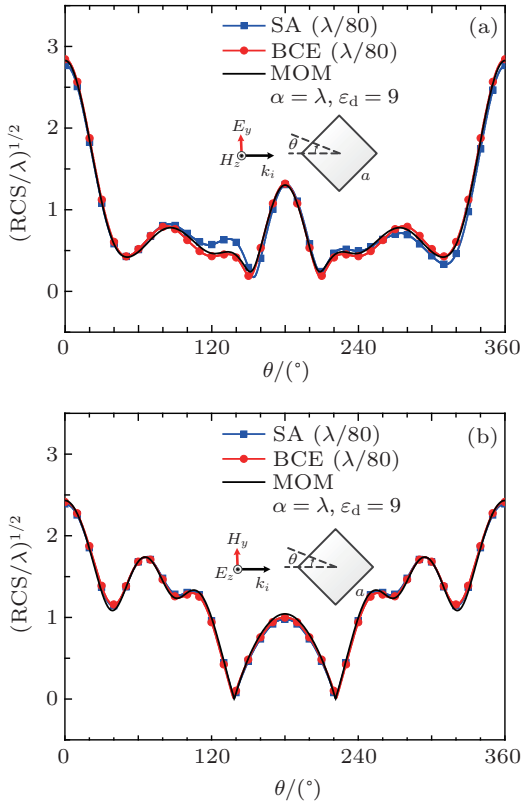



**Fig. 9.** (color online) Far field RCS comparison ($a = \lambda$, $\varepsilon_{\rm d} = 9$). SA and BCE are staircase approximation and boundary condition equations methods. (a) TE wave illumination and (b) TM wave illumination.

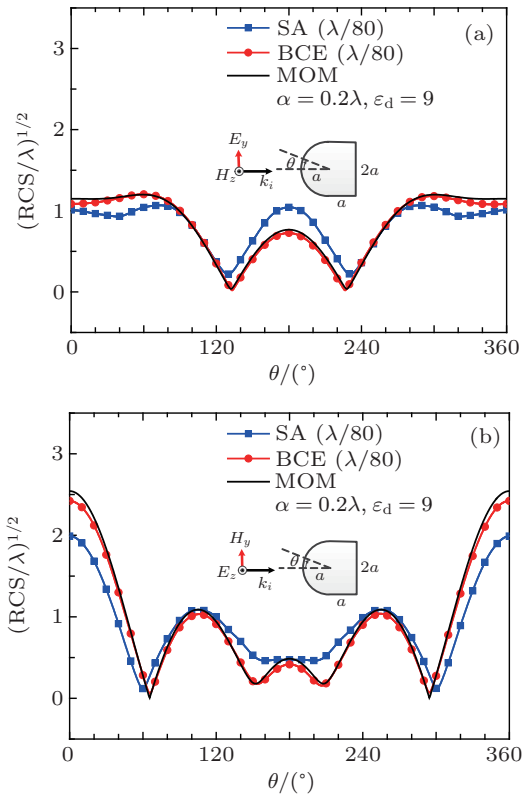



**Fig. 10.** (color online) Far field RCS comparison ($a = 0.2\lambda$, $\varepsilon_{\rm d} = 9$). SA and BCE are staircase approximation and boundary condition equations methods. (a) TE wave illumination and (b) TM wave illumination.

Figures 9 and 10 show the BCE method predicted RCS and the SA method predicted RCS compared with the results of the MOM method. Obviously, the results of the BCE method agree well with those of the MOM method for both TE and TM wave illuminations, whereas the results of the SA method with a grid size of $\lambda/80$ do not agree well with that of the MOM method for TE wave illumination. The reason is that the sloped surfaces on the square cylinder will introduce a staircase error in the FDTD simulation.[19] The BCE method is able to eliminate the staircase approximation error and restore the second-order accuracy in FDTD simulations.

## 4. Conclusion

The BCE method is proposed to deal with the curved surface scattering in the FDTD calculation. In this method, the curved surface interfaces are modeled by adding the boundary condition equations. Thus, the real shapes of a curved surface can be simulated and the staircase approximation errors can be eliminated. To validate the BCE method, various scattering properties are analyzed, including the induced surface current of a PEC circular, and the near field and far field scattering of the dielectric cylinders. The results show that the BCE method can maintain a second-order accuracy by eliminating the staircase approximation error effectively, whereas the SA and AM methods can only achieve a first-order accuracy. The results of the BCE method show better accuracy than that of the SPS method by considering the physical location of curved surfaces according to the surface location and intersection ratio. In addition, the results of the BCE method agree well with those of the analytical solution method for different dielectric contrast cases.

## References


[1] Warnick K F and Chew W C 2001 *Waves Random Media* **11** R1
[2] Jin L, Zhu Q Y, Fu Y Q and Yu W X 2013 *Chin. Phys. B* **22** 104101
[3] Li J, Guo L X, Zeng H and Han X B 2009 *Chin. Phys. B* **18** 2757
[4] Li Q B, Wu R X, Yang Y and Sun H L 2013 *Chin. Phys. Lett.* **30** 074208
[5] Liang C, Xu Y M and Wang Z J 2008 *Chin. Phys. Lett.* **25** 3712
[6] Zhan C L, Ren X F, Huang Y F, Duan K M and Guo G C 2008 *Chin. Phys. Lett.* **25** 0559
[7] Lou S, Tsang L, Chan C and Ishimaru A 1990 *Microw. Opt. Technol. Lett.* **3** 150
[8] Hastings F D, Schneider J B and Broschat S L 1995 *IEEE Trans. Antennas Propagal.* **43** 1183
[9] Lou S, Tsang L and Chan C 1991 *Waves Random Media* **1** 287
[10] Krause K, Lou S, Tsang L and Chan C 1991 *Microw. Opt. Technol. Lett.* **4** 255
[11] Devayya R and Wingham D 1992 *IEEE Trans. Geosci. Remote Sensing* **30** 645
[12] Tsang L, Lou S and Chan C 1991 *Microw. Opt. Technol. Lett.* **4** 527
[13] Taflove A and Hagness S C 2005 *Computational Electrodynamics* (Artech House)
[14] Elsherbeni A Z and Demir V 2009 *The Finite-difference Time-domain Method for Electromagnetics with MATLAB Simulations* (Raleigh, NC: SciTech Pub)
[15] Liu S B and Liu S Q 2004 *Chin. Phys.* **13** 1892
[16] Shen J, Sha W, Huang Z X, Chen M S and Wu X L 2012 *Acta Phys. Sin.* **61** 190202 (in Chinese)
[17] Liu Y W, Chen Y W, Zhang P and Liu Z X 2014 *Chin. Phys. B* **23** 124102
[18] Schneider J B and Shlager K L 1997 *IEEE Trans. Antennas Propagal.* **45** 1830
[19] Mohammadi A, Nadgaran H and Agio M 2005 *Opt. Express* **13** 103671
[20] Hao Y and Railton C J 1998 *IEEE Trans. Microwave Theory Tech.* **46** 82
[21] Fusco M 1990 *IEEE Trans. Antennas Propagal.* **38** 76
[22] Jurgens T, Taflove A, Umashankar K and Moore T 1992 *IEEE Trans. Antennas Propagal.* **40** 357
[23] Railton C J, Craddock I and Schneider J B 1995 *Electron. Lett.* **31** 1585
[24] Kosmanis T and Tsiboukis T D 2003 *IEEE Trans. Microwave Theory Tech.* **51** 839
[25] Oskooi A F, Kottke C and Johnson S G 2009 *Opt. Lett.* **34** 2778
[26] Liu D C and Chang H C 2012 *IEEE Trans. Antennas Propagal.* **60** 5259
[27] Farjadpour A, Roundy D, Rodriguez A, Ibanescu M, Bermel P, Joannopoulos J, Johnson S G and Burr G 2006 *Opt. Lett.* **31** 2972
[28] Kottke C, Farjadpour A and Johnson S G 2008 *Phys. Rev. E* **77** 036611
[29] Ditkowski A, Dridi K and Hesthaven J S 2001 *J. Comput. Phys.* **170** 39
[30] Xiao T and Liu Q H 2004 *IEEE Trans. Antennas Propagal.* **52** 730
[31] Jackson J D 1962 *Classical Electrodynamics* (New York: Wiley)
[32] Hwang K P and Cangellaris A C 2001 *IEEE Microw. Wirel. Compon. Lett.* **11** 158
[33] Balanis C A 2012 *Advanced Engineering Electromagnetics* (Vol. 111) (Wiley Online Library)
[34] Bourlier C, Pinel N and Kubické G 2013 *Method of Moments for 2D Scattering Problems: Basic Concepts and Applications* (John Wiley & Sons)
[35] Harrington R F 1961 *Time-harmonic Electromagnetic Fields* (McGraw-Hill)
[36] Kerker M 1969 *The Scattering of Light* (New York: Academic Press)
[37] Bohren C F and Huffman D R 2008 *Absorption and Scattering of Light by Small Particles* (John Wiley & Sons)